Turunen, Konsta; Yazdani, Maryam Roza; Puupponen, Salla; Santasalo-Aarnio, Annukka; Seppälä, Ari

Cold-crystallizing erythritol-polyelectrolyte

Published in:
Applied Energy

DOI:
10.1016/j.apenergy.2020.114890

Published: 15/05/2020

Document Version
Publisher's PDF, also known as Version of record

Applied Energy 266 (2020) 114890

Contents lists available at ScienceDirect

Applied Energy

journal homepage: www.elsevier.com/locate/apenergy

Cold-crystallizing erythritol-polyelectrolyte: Scaling up reliable long-term heat storage material

Konsta Turunen, Maryam Roza Yazdani, Salla Puupponen, Annukka Santasalo-Aarnio, Ari Seppälä*

Department of Mechanical Engineering, School of Engineering, Aalto University, P.O. Box 16100, 00076 Aalto, Finland

HIGHLIGHTS

- Demonstrating 97-day TES using cold-crystallizing material in bulk size (160 g).
- Over 70% of latent heat can be stored without losses for at least three months.
- High-erythritol composition showed high heat storage capacity of 250 MJ/m^3.
- Maximum heat release temperature at above 80 °C by adjusting composition.
- Optimized compositions indicate sufficient heat release rate for applications.

GRAPHICAL ABSTRACT

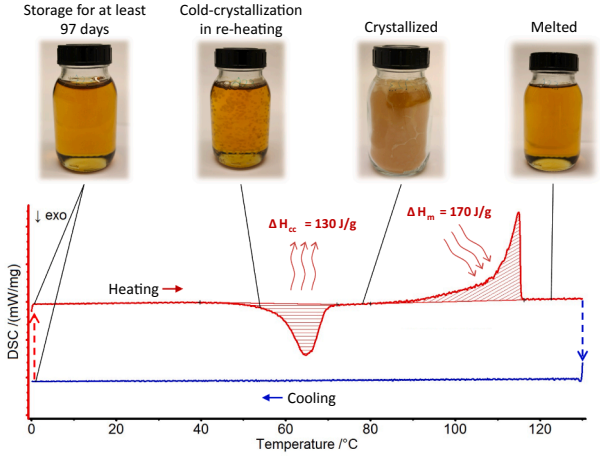

ARTICLE INFO

Keywords:
Long-term thermal energy storage
Phase change material
Supercooling
Cold-crystallization
Erythritol

ABSTRACT

Renewable energy usage would benefit from efficient and high-capacity long-term heat storage material. However, these types of material solutions still lack reliable and durable operation on bulk level. Previously, we showed that cold-crystallizing material (CCM), which consists of erythritol in cross-linked polymer matrix, stored heat for a long-term period in a milligram scale by supercooling stably and preventing undesired crystallization during storage. Crystallization of CCM can be triggered efficiently by re-heating the material (i.e. cold-crystallization). Supercooling and cold-crystallization are stochastic phenomena which manifest in a way that the properties in bulk scale often deviate from the microscale. In this work, we scale up CCM to a bulk size of 160 g, and analyze its supercooling and crystallization characteristics for long-term heat storage. In order to identify the impact of the scale-up on the tested compositions and to discover optimal storage conditions, CCM samples are maintained in storage mode at constant temperature between 0 and 10 °C and up to 97 days. To this end, the thermal chamber measurement procedure estimates the heat release of CCM samples based on the measured temperature data and the one-dimensional transient heat conduction model. Results indicate that the heat release in cold-crystallization is over 70% of the melting heat. This heat can be stored without reduction for at least 97 days, demonstrating the reliable performance of long-term heat storage. Analysing the thermal properties of CCM compositions indicates a maximum volumetric storage capacity of 250 MJ/m^3 and excellent properties for further heat storage applications.

* Corresponding author.
E-mail address: ari.seppala@aalto.fi (A. Seppälä).

https://doi.org/10.1016/j.apenergy.2020.114890
Received 24 September 2019; Received in revised form 28 February 2020; Accepted 22 March 2020

Nomenclature

A	Surface area (m^2)
a	Thermal diffusivity (m^2/s)
Bi	Biot number (–)
CCM	Cold-crystallizing material
C_p	Specific heat (J/g K)
DSC	Differential scanning calorimetry
h	Enthalpy (J/g)
k	Thermal conductivity (W/m K)
L_k	Characteristic length (m)
m	Mass (g)
PAANa	Partly neutralized polyacrylic acid or sodium polyacrylate
PCM	Phase change material
q	Heat flux (W/m^2)
s	Thickness (m)
SAT	Sodium acetate trihydrate
T	Temperature (°C)
T_{max}	Maximum temperature during cold-crystallization (°C)
t	Time (s)
TES	Thermal energy storage
V	Volume (m^3)
W	Mass fraction (–)
X	Molar neutralization degree of PAANa (%)

Greek letters

α	Heat transfer coefficient (W/m^2 K)
ΔH	Latent heat (J/g)
Δt	Duration of time step (s)
ε_{sto}	Storage efficiency (–)
ρ	Density (kg/m^3)

Subscripts

c	Container
cc	Cold-crystallization
CCM	Cold-crystallizing material
d	Down section of the heat conduction model
ery	Erythritol
g	Glassy state
i	Container-insulation boundary (inner boundary)
j	Number of a time step
l	Liquid
m	Melting
o	Measurement point in the insulation shell (outer boundary)
PAANa	Partly neutralized polyacrylic acid or sodium polyacrylate
s	Solid
sd	Side section of the heat conduction model
sil	Silicon oil
sto	Storage
u	Up section of the heat conduction model
w	Weighed while suspended in silicon oil
0	Reference point

1. Introduction

Solar energy suffers from an intermittent production profile that varies on a diurnal and seasonal basis. For example, in Nordic countries, solar irradiation is abundant in summer, and scarce in winter when heat demand is high. Therefore, excess production ought to be stored during the summer months and used to cover peak heat production in winter. In order to solve this issue, long-term thermal energy storage (long-term TES) is an attractive technology for balancing the mismatch between the seasons and increasing system reliability.

TES can be classified into three categories based on the way heat is stored: sensible heat, latent heat and thermochemical storage. Current long-term TES systems rely on large sensible heat storages, in which heat is stored by increasing the temperature of the storage medium. Therefore, typical storages, such as water tanks and boreholes [1], are located underground. These storages require large amount of space because of continuous heat loss during the storage period. Storing heat in this manner has a large investment cost, because it is expensive to undertake large-scale excavation and create insulation for large volumes [2].

In contrast to sensible heat, thermochemical heat is a promising method for the long-term heat storage, because it often exhibit high energy densities and, potentially, a minimal loss of heat [3]. Typically, heat is stored in a reversible chemical reaction or a sorption process, where for example water vapor is adsorbed and desorbed. Recently, researches have extensively studied the sorption processes [4]. However, this method has not yet been commercialized because of the barriers in material development, such as poor thermal stability, high cost and inconsistent cycling behavior [3,4].

The third way of storing heat employs phase change materials (PCMs), which can store a large amount of thermal energy in the form of latent heat. This is most commonly during the melting and crystallization of PCMs. Latent heat storage systems also suffer from heat loss during storage, cooling the PCM. When PCMs cool below its equilibrium melting temperature (T_m), it crystallizes and releases heat, or it supercools and remains in a liquid phase, thus it is in a metastable state [5]. Traditionally, supercooling is undesired in TES because solidification does not begin when T_m is achieved. Nevertheless, latent heat can be stored for several years without heat loss in the supercooled state, if spontaneous crystallization does not occur [6]. Further research on the supercooling of PCMs may be found in review articles [7] and [8].

Supercooling has been utilized in small-scale TES since 1895 [9]. Currently, it is employed in commercial heating pads [10], where supercooled sodium acetate trihydrate (SAT) stores heat until crystallization is initiated. SAT has a high melting heat (ΔH_m = 265 J/g) and melting temperature of 58 °C [11], which is suitable for low-temperature applications. Large-scale and long-term storing of heat in 100–200 kg SAT storage units revealed unreliable operation due to metastability of supercooled SAT [12,13,14]. Nonetheless, research continues to attempt to overcome these challenges concerning metastability [14]. Probability of nucleation in supercooled liquid increases when sample volume grows and factors such as impurities, rough surfaces, and pressure changes may initiate spontaneous crystallization [15]. Supercooling behavior of other materials, such as disodium hydrogen phosphate dodecahydrate (DSP) [6,16] and polyols [17,18,19,20] have been also explored for supercooled TES, but they face the same difficulties as SAT with concern over metasatbillity or the initiation of crystallization is inefficient.

In addition to supercooled state, other metastable states have been adopted for long-term TES. A recent investigation analyzed photoswitching materials, which undergo transformation from a stable state into a higher energy level metastable isomer by light. Heat release is initiated via catalyst or heat [21]. Heat release of 277–559 J/g and storage half-life up to 48.5 days in milligram scale has been documented [22], but optimizing absorption in the spectrum of sun light is still ongoing. Photoswitches are also applied to dope existing organic PCMs, in order to improve stability against crystallization, but thus far, gradual crystallization has been observed after 10 h of storage [23]. For Schiff-base nickel complexes, undesired crystallization has been prevented by cooling the melt (T_m ~ 290 °C) below its glass transition

temperature (T_g), and heat is released by crystallizing the material on the subsequent heating, that is in cold-crystallization [24]. High operating temperature limits the applications of the material, and knowledge on long-term stability for melting-crystallization cycling is still required.

Recent research in applying supercooled and other metastable states for TES is a call for advanced long-term TES solutions with high storage capacity. To date, researches have not yet been able to find the most reliable method for these solutions on a bulk scale for long-term storage in terms of months. We previously developed cold-crystallizing material (CCM), which consisted of erythritol dispersed in sodium polyacrylate matrix [19]. The operational principle of CCM is based on supercooling and cold-crystallization. When supercooled CCM is cooled, its molecular movement slows down. Eventually, the movement becomes so slow that the liquid acts as an amorphous solid, or a glass. Therefore, spontaneous crystallization can be avoided. Characteristically, the supercooled liquid has to be cooled down fast to reach a glassy state without crystallization. Nevertheless, polyols have many stable local conformations, which differ from the crystal structure. These conformations have large activation energy for the molecular rearrangement. This, together with strong ion-dipole interactions between the polyol and the polymer, prevent crystallization of supercooled CCM even at slow cooling rates (0.05 K/min) [19]. When CCM is re-heated from a glassy state, molecular movement increases, allowing relaxation to the crystal structure, that is cold-crystallization. In our previous study [19], CCM showed long-term heat storing ability up to one month, melting heat of 150–260 J/g and a suitable melting temperature of 95–110 °C for domestic heating purposes on a milligram scale.

The probability of nucleation in supercooled liquid increases when the sample volume grows, thus the confirmed supercooling behavior of previously examined CCM compositions in a milligram scale cannot be guaranteed in a bulk scale. Therefore, this paper analyzes heat release properties and supercooling stability of CCM with 160-g samples and identifies optimal compositions for long-term TES applications. As the glass transition temperature of CCMs is low ($T_g < 0$ °C), measurements examine the samples in a deeply supercooled liquid region at the storage temperatures of 0 °C, 5 °C and 10 °C, in order to define optimal storage conditions for different compositions. To this end, the thermal chamber measurement procedure estimates cold-crystallization heat (released heat content) of the stored sample by implementing the measured temperature data in the one-dimensional transient heat conduction model. The results indicate that heat can be reliably stored over a three-month period without a decrease in released latent heat. In addition to bulk scale analysis, the study also measured thermal properties and the density of CCM.

2. Materials and methods

2.1. Material preparation

The main components of CCM are ertyhritol (technical grade, supplied by Suomen Luontaistukku Ltd., Finland) and sodium polyacrylate (PAANa). PAANa was prepared by polymerizing acrylic acid (assay ≥ 99%, supplied by Merck) neutralized with sodium hydroxide (assay ≥ 99%, supplied by VWR Chemicals). Ethylene glycol dimethacrylate (assay ≥ 97.5%, supplied by Merck) was used as cross-linking agent and potassium persulfate (assay ≥ 98%, supplied by VWR Chemicals) as a polymerization initiator. Preparation of CCM follows the method used by Puupponen and Seppälä [19].

Supercooling and cold-crystallization properties of CCM were altered by changing the mass fraction of ertyhritol (W_{ery}) and the neutralization degree of PAANa (X). Table 1 lists the studied compositions and the altered parameters W_{ery} (0.75 or 0.8) and X (0.85 or 1). Mass fraction of ethylene dimethacrylate and potassium persulfate remained constant for all compositions at 0.02 and 0.001, respectively. Prepared CCM batches were divided into 160 ± 5 g samples. Two batches of each composition were prepared and each batch was divided into at least two samples.

Table 1
The amount of each component in the tested CCM compositions. In addition to the listed materials, all compositions contained 2 wt-% ethylene dimethacrylate and 0.1 wt-% potassium persulfate.

Composition name	Erythritol mass fraction, W_{ery}	PAANa molar neutralization degree, X	PAANa mass fraction, W_{PAANa}
A	0.8	1.0	0.179
B	0.75	1.0	0.229
C	0.75	0.85	0.229

2.2. Thermophysical properties analysis

Resulting from the size-dependent behaviour of supercooling, thermal properties of CCM were analysed in small-scale (sample size 15–30 mg) using differential scanning calorimetry (Netzsch DSC204F1 Phoenix DSC) and in bulk scale (sample size 160 g) using the thermal chamber measurement procedure (Section 2.3.3). Two types of DSC measurement programs were used in the characterization. The first measurement program was used to determine melting, crystallization and glass transition properties of CCM. It consisted of four consecutive heating-cooling cycles between −60 °C and 130 °C using a scan rate of 0.5 K/min. The onset values during heating were used to determine cold-crystallization temperature (T_{cc}) and T_m, but glass-transition temperature (T_g) was determined by the onset value during cooling. Specific heat of CCM was determined with the second measurement program, where four heating-cooling cycles between −60 °C and 130 °C were used with a scan rate of 5.0 K/min. The average values from three heating-cooling cycles were used in the analysis, and at least four parallel samples were measured for each composition.

C-Therm TCI equipment was applied for measuring thermal conductivity with a modified transient source plane technique. Three cylindrical discs made of solid phase CCM-A samples with diameter of 62 mm and height of 12 mm were prepared. For minimizing any contact problems between the sample and the sensor, the samples were carefully polished, and 200 µl of silicon oil was applied as a contact material. The equipment was calibrated first with water, followed by polystyrene, pyrex, PVC and pyroceram. Silicon oil was used as the contact material. Based on the calibration, measurement accuracy was estimated to be 4%.

Density of CCM was measured using the displacement method, where the mass of the CCM sample was first measured in atmospheric conditions. Then, it was measured being suspended in silicon oil with fine line. Based on the density of silicon oil, density of CCM was calculated as follows: $\rho_{CCM} = \rho_{sil} m_{CCM} / m_{CCM,w}$. ρ_{sil} is the density of the silicon oil and subscript w refers to being suspended in silicon oil. The average of 12 CCM-A samples (8–9 g) from two batches was measured in supercooled and solid states. The method was first verified by measuring the density of pyrex and pyroceram, which indicated a maximum deviation of 1% from the calibration values.

2.3. Scale-up measurement procedure

The purpose of the scale-up measurements was to find bulk scale compositions that have high cold-crystallization heat and remain stable against spontaneous crystallization for months. However, scaling up is not a straightforward task because the probability of nucleation in supercooled liquid increases as the sample volume grows. Therefore, we first selected the most suitable CCM compositions by scale-up experiments. Then, the heat storing capability of CCM (with optimized composition) was measured using 160 g samples in a two-stage measurement procedure consisting of a storage stage and a thermal chamber measurement stage.

2.3.1. Composition selection

In storage mode, CCM is in deeply supercooled liquid (close to T_g) or glassy state. The aim is to store the latent heat of CCM in as high a temperature as possible without compromising the stability against spontaneous crystallization, for example in a deeply supercooled liquid state. Above the glass transition temperature (T_g), the glassy substance converts to a supercooled liquid. At the same time, molecular movement increases in the deeply supercooled liquid, increasing the possibility of nucleation. When heating is continued, nuclei will eventually occur and crystals will begin to form, but the kinetics of crystallization determine the overall speed of the crystallization. Therefore, increasing T_g of the material provides improved stability at higher temperatures. As shown in our previous research [19], the increase in T_g can be achieved by decreasing the mass fraction of polyol and increasing the neutralization degree of sodium polyacrylate, because both factors reinforce the interactions between the polyol and the polymer. Simultaneously, crystallization kinetics may slow down and cause melting heat to decrease, because of an increased fraction of non-freezing bound polyol.

The most potential CCM compositions were identified by scale-up experiments before studying the heat storage performance of CCM in 160 g scale. Several compositions consisting of various mass fractions of erythritol and molar neutralization degrees of PAANa were tested in two-stage scale-up. The aim was to identify compositions that show stable supercooling during cooling to 0 °C and distinctive cold-crystallization behavior. Fig. 1 shows the values of the examined parameters at each stage of the scale-up and our previously reported values [19]. In the first stage (Cold-crystallization), we tested the occurrence of cold-crystallization in a 20 g sample size by measuring the temperature of the sample when cold-crystallization was expected, for example during heating from a deeply supercooled state from 0 °C to 60 °C (T_m ~ 106–108 °C, see Table 5). Samples that did not show evident temperature increase (tens of degrees) during cold-crystallization were excluded from the second stage of the scale-up. During the second stage (Supercooling stability), stability against spontaneous crystallization was studied by visually observing crystallization with 20–30 samples (m ~ 0.5 g) which were slowly cooled from their melting temperature to a deeply supercooled state. Finally, three stable compositions (A, B and C, listed in Table 1) were chosen for the 160 g scale study. In order to enhance stability at above 0 °C, we increased the neutralization degree of PAANa as the scale-up progressed, as can be seen in Fig. 1. Reduction of eryhtritol mass fraction also increases the stability of CCM. However, we chose to retain the mass fractions at 75 wt-% and 80 wt-%, in order to ensure a high melting heat and sufficient crystallization kinetics.

2.3.2. Storage conditions

Supercooling and crystallization behavior of 160 g CCM samples was examined with stability and cycling measurements. Table 2 lists the storage conditions for both measurement types and compositions. Each storage condition for the tested composition was measured using two parallel samples. CCM samples are referred as “a-b-c”, where “a” refers to the composition (A, B or C), “b” to the storage temperature (0, 5 or 10) and “c” to the batch number (1 or 2).

Stability measurements tested the stability of supercooled liquid state, when supercooled samples were kept at 0 ± 1.5 °C, 5 ± 1.5 °C and 10 ± 1.5 °C storage temperature. The storage period varied between one and 97 days, as indicated in Table 2. We chose the storage temperature to be as high as possible, but low enough to prevent spontaneous crystallization of supercooled samples, in order to find optimal storage conditions for each composition. Colder storage temperatures would improve the stability of the CCM, but it would also be harder to implement in real-life applications. Given the long duration of the measurement procedure, two storage temperatures were tested for each composition. Fig. 2 shows an example of the temperature program and the sample temperature during an entire measurement cycle. The storage stage began by melting a sample in an oven at 130 °C and cooling it to 0 ± 1.5 °C in a refrigerator, in order to ensure similar thermal history of the samples, as seen in Fig. 2. Next, the supercooled sample was placed in a refrigerator at the specified storage temperature and kept there for the storage period. After the storage period ended, the cold-crystallization was initiated using a thermal chamber setup, which is described in Section 2.3.3.

Thermal cycling stability of CCM-A was examined by subsequently melting and crystallizing the sample 50 times in cycling measurements. The sample was first melted in an oven at 130 °C and then cooled to the storage temperature of −20 ± 2.0 °C. After a one-day storage period, the sample was crystallized in an oven at around 80 °C and the melting-crystallization cycle re-initiated, except for every tenth cycle, when the cold-crystallization heat was measured using a thermal chamber setup.

2.3.3. Thermal chamber measurement procedure

The cold-crystallization heat of the 160 g CCM samples was determined by applying experimental temperature data from thermal chamber measurement setup in a transient one-dimensional heat conduction model. The setup consists of a sample container, which is inserted in an insulation shell (Fig. 3a). During the measurement, the shell with a sample was placed inside a temperature-controlled chamber (Fig. 3b). J-type thermocouples measured temperatures in 11 positions (shown in Fig. 3a). The measurement began by heating the supercooled sample (T = 0–10 °C) with a constant temperature (T = 50–65 °C) in the chamber, as is shown in Fig. 2. Heating initiated the cold-crystallization process, which increased the sample temperature abruptly above the chamber temperature (see Fig. 2). After the abrupt temperature increase, the sample was cooled back to the cold-crystallization temperature by another constant temperature step in the chamber. Due to the different cold-crystallization properties, temperature programs differed between the compositions, as shown in Table 3. Duration and temperature of the isothermal steps were chosen based on the DSC measurements. After the measurement, the sample was completely crystallized. Therefore, one measurement with the thermal chamber measurement procedure can estimate cold-crystallization heat for only one specific storage condition. Indeed, an individual measurement procedure is necessary for each storage condition.

A one-dimensional heat conduction model was used to determine a temperature distribution between the measurement point at the container-insulation boundary and the point inside the insulation shell (Fig. 3a). The model consisted of three sections: side (sd), up (u), and

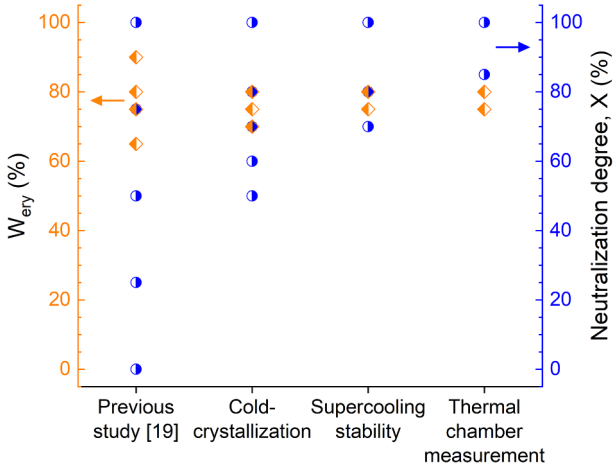

Fig. 1. Investigated mass fraction of erythritol (W_{ery}) and neutralization degree of sodium polyacrylate (X) during each stage of scale-up experiments and our previously studied values [19]. The studied W_{ery} values are marked as orange diamonds and X values as blue spheres. Thermal chamber measurement refers to the 160 g samples researched in more detail.

Table 2
Storage conditions for testing stability and thermal properties of CCM compositions in thermal chamber measurement procedure. Measurements are divided into two groups: stability measurements, where storage temperature and storage period are changed, and cycling measurements, where every tenth melting-crystallization cycle is measured when storage temperature and period are kept constant.

Measurement type	Stability measurements														Cycling measurements					
Storage variable	Storage period (days)														Number of cycle (–)					
Storage temperature (°C)	0					5					10				−20					
Composition A	1	10	30	57	97	1	10	30	57	97					1	10	20	30	40	50
Composition B	1	10	30		97	1	10	30		97										
Composition C						1	10	30		97	1	10	30	97						

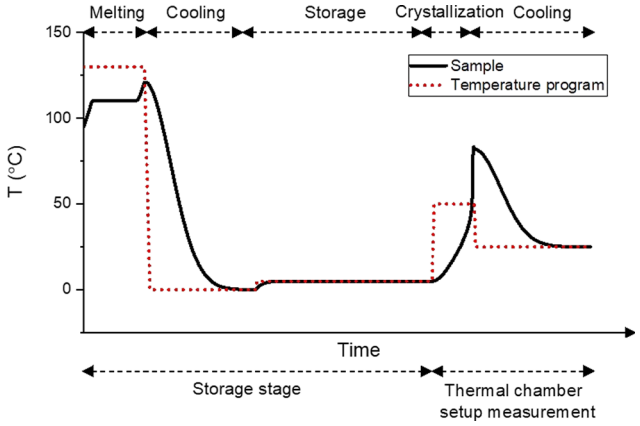

Fig. 2. An example of the temperature program and the sample temperature during one thermal chamber measurement procedure. The measurement is divided into two stages: storage stage, when sample is melted, cooled and heat is stored; and thermal chamber setup measurement stage, when sample cold-crystallizes and released heat is estimated.

down (d). These sections were allocated in order to improve the accuracy of the model. Furthermore, the side section of the model used the average of three measurement points at the container-insulation boundary and inside the shell. The temperature distribution was determined by solving the heat equation: Eq. (1) for heat conduction along the r-axis and Eq. (2) for the z-axis. The equations were discretized using the control volume approach. For this approach, 90 control volumes with length of 0.2 mm were implemented for each section of the model. Maximum absolute changes of 10^{-4} °C for the temperature of a control volume and time step of 10 s were applied in

Table 3
Temperature programs of the oven in thermal chamber measurements for each of the tested compositions.

Composition	Heating (1. step)	1. Isothermal (2. step)	Cooling (3. step)	2. Isothermal (4. step)
A	5 K/min	50 °C / 6 h	5 K/min	22 °C/~10 h
B	5 K/min	55 °C/6 h	5 K/min	25 °C/~8h
C	5 K/min	65 °C/8 h	5 K/min	35 °C/~8h

the iteration. Measured temperatures were set as the time-dependent boundary conditions as described in Eqs. (3)–(8):

$$\frac{\partial T}{\partial t} = a\left(\frac{\partial^2 T}{\partial r^2} + \frac{1}{r}\frac{\partial T}{\partial r}\right) \quad (1)$$

$$\frac{\partial T}{\partial t} = a\left(\frac{\partial^2 T}{\partial z^2}\right) \quad (2)$$

$$T_{sd,i}(t) = T(r = r_i, z = 0, t) \quad (3)$$

$$T_{sd,o}(t) = T(r = r_o, z = 0, t) \quad (4)$$

$$T_{u,i}(t) = T(r = 0, z = 0.05m, t) \quad (5)$$

$$T_{u,o}(t) = T(r = 0, z = 0.068m, t) \quad (6)$$

$$T_{d,i}(t) = T(r = 0, z = -0.05m, t) \quad (7)$$

$$T_{d,o}(t) = T(r = 0, z = -0.068m, t) \quad (8)$$

where a is thermal diffusivity (m^2/s); and subscripts i and o refer to container-insulation boundary and measurement point in the insulation, respectively.

The heat conduction model was used to estimate the temperature

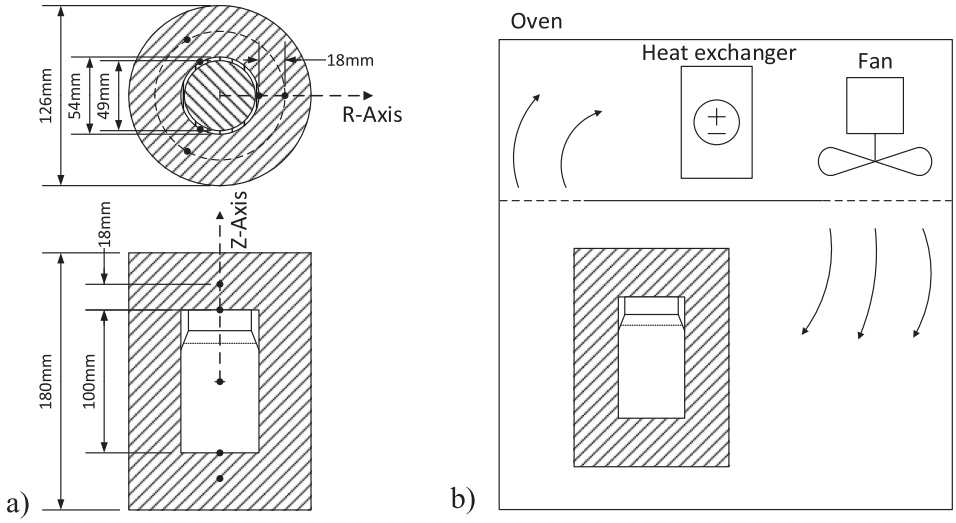

Fig. 3. The schematic of the thermal chamber measurement setup: (a) Dimensions of a sample container and insulation shell. Locations of the thermocouples are marked with black dots. (b) Setup for heating and cooling the CCM sample during thermal chamber measurement, when predetermined temperature program is run.

gradient at the container-insulation interface for each section. Consequently, the heat flux, q (W/m^2), at the interface was calculated based on the temperature gradient. The enthalpy-temperature curve of the sample during the measurement was then formed according to Eqs. (9)–(11).

$$h(T_{CCM}) = h_0 + \sum dh_j \tag{9}$$

$$dh_j = \frac{1}{m_{CCM}}[(A_{sd}q_{sd}(t_j) + A_u q_u(t_j) + A_d q_d(t_j))\Delta t - m_c C_{p,c}(T_{sd,i}(t_j) - T_{sd,i}(t_{j-1})) - m_{lid} C_{p,lid}(T_{u,i}(t_j) - T_{u,i}(t_{j-1}))] \tag{10}$$

$$T_{CCM}(t_j) = \frac{T_{sd,i}(t_j) + T_n(t_j)}{2} \tag{11}$$

where, h is enthalpy (J/g), h_0 enthalpy of the CCM at the beginning of the measurement, A heat transfer area, q heat flux (W/m^2), c_p specific heat, T_n temperature at the middle of CCM sample and T_{CCM} average temperature of the sample. Subscript j refers to a time step and c to container. The properties of the materials used in the thermal chamber measurement setup and data analysis are listed in Table 4.

Accuracy of the described method was confirmed by uncertainty analysis and validation measurements. Uncertainty of measured parameters was experimentally estimated by following the Guide to the expression of uncertainty in measurements [25]. For mass and thickness measurements, rectangular distribution with 95% level of confidence was applied yielding an expanded uncertainty of ± 0.0095 g and ± 0.024 mm, respectively. For the temperature, normal distribution was used, as measured temperature calibration data was available. For 95% level of confidence, expanded uncertainty resulted in ± 0.06 °C. The validation measurements were conducted by measuring the melting heat and the temperature of the de-ionized water and tetradecanoic acid (assay ≥ 98%, supplied by VWR Chemicals). For water, the reference value of the melting heat is 334.0 J/g and the melting temperature 0.0 °C, and for tetradecanoic acid, these values are 198.7 J/g and 53.9 °C, respectively [26]. The measurements were repeated three times for both materials and they showed maximum deviation of 3% for melting heat and 0.3 °C for melting temperature from the literature values [26].

Fig. 4 shows an example of the enthalpy-temperature curve for the cold-crystallization measured with the thermal chamber setup. The dashed line illustrates the cold-crystallization process of the sample, if the temperature increase during the cold-crystallization would be adiabatic. Since the specific heat of liquid state is larger than in a solid state, we can find a maximum value for an enthalpy difference between the liquid (or partially solid) state and the solid state in the curve, that is, between the temperature increasing and decreasing part of the curve. In the adiabatic crystallization case, the maximum value (ΔH_{max}) is located at the beginning of cold-crystallization (T_{cc}) because a liquid phase has a larger specific heat than a solid phase. During crystallization the enthalpy remains constant. Heat release during cold-crystallization (ΔH_{cc}) can be then defined as the enthalpy difference between the point where cold-crystallization begins and the point where crystallized sample has cooled back to T_{cc}, which is ΔH_{max}. In reality, sample receives some heat from the environment after T_{cc} has been reached, which can be seen in Fig. 4 as measurement data reaches higher enthalpy values than the adiabatic crystallization curve.

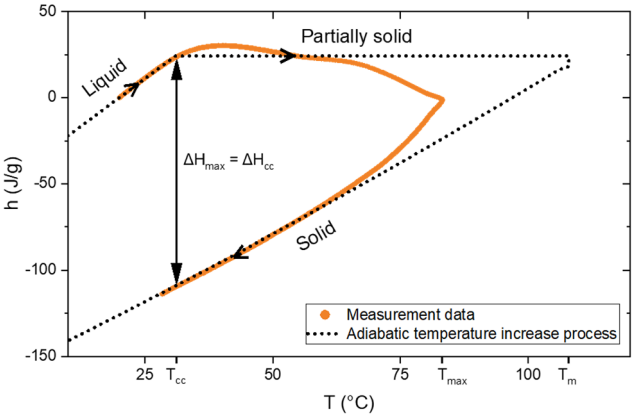

Fig. 4. Enthalpy-temperature curve for a measured cold-crystallization of CCM and an approximate process, where temperature increase during cold-crystallization is adiabatic. The reference point of enthalpy is liquid at T = 20 °C, p = 1 bar. Cold-crystallization heat and temperature can be found by determining the maximum change of enthalpy between the temperature increasing and decreasing part of the curve.

However, this has a negligible effect on the analysis because crystallization rate is fast and the temperature of the oven is set close to T_{cc}. Therefore, the above described method is used to determine T_{cc} and ΔH_{cc}.

A Biot number (Bi) describes the suitability of assuming that the entire sample is at uniform temperature during the measurement. It is defined as; $Bi = \propto L_k/k$, where $\propto$ is the heat transfer coefficient between the material and environment and $L_k = V/A$ is the characteristic length. Typically, when Bi < 0.1, the assumption is valid. Because convective heat transfer resistance between the insulation and air is significantly smaller than conductive resistance in the insulation shell, the overall heat transfer coefficient between the air and outer boundary of the CCM sample is simplified to $\propto = k/s$. Based on the measured thermal conductivity of CCM-A (liquid 0.35 W/m K and solid 0.77 W/m K, see Table 5), we estimated that Bi 0.02⋯0.03.

Another way of determining thermal properties of PCM in bulk size is to use T-history method developed by Yingping et al. [28]. In order to ensure uniform temperature of the sample and minimizing errors due to setup configuration, it has been recommended to insulate the sample in T-history measurement [29]. However, ignoring the thermal mass of the insulation has been shown to lead into systematic errors in forming enthalpy-temperature curves [30,31]. Since temperature increases abruptly during cold-crystallization and we wanted to ensure uniform temperature of the sample by insulation, we did not use the traditional T-history method in this research.

3. Results and discussion

3.1. Thermophysical properties of CCM

Table 5 lists the melting and the crystallization properties of CCM measured with DSC, thermal conductivity and density. The highest melting heat (ΔH_m = 173 J/g) is achieved for CCM-A, which has the

Table 4
Properties of the materials used in thermal chamber measurement procedure and heat transfer analysis.

Material	Mass (m) [g]	Density (ρ) [kg/m^3]	Specific heat (C_p) [J/g K]	Thermal conductivity (k) [W/m K]
Armaflex XP (insulation)		75	1.35*	0.04
Glass (container) [27]	115.40 ± 0.30	2500	0.75	1.00
Polypropylene (lid) [27]	4.00	910	1.80	0.22

* Measured using DSC.

Table 5
Thermophysical properties of CCM with standard deviation. Subscript l refers to liquid, s to solid and g to glassy state.

Measurement type	Property	Unit	CCM-A	CCM-B	CCM-C
DSC	T_m	°C	108 ± 1	106 ± 1	108 ± 1
	ΔH_m	J/g	173 ± 3	138 ± 8	151 ± 4
	T_{cc}	°C	48 ± 4	56 ± 5	59 ± 3
	ΔH_{cc}	J/g	128 ± 5	109 ± 8	110 ± 3
	T_g	°C	−18 ± 4	−10 ± 2	−6 ± 2
	$C_{p,l}$ (T = 130 °C)	J/gK	2.53 ± 0.08		2.49 ± 0.07
	$C_{p,l}$ (T = 20 °C)	J/gK	2.16 ± 0.04		2.14 ± 0.03
	$C_{p,s}$ (T = 50 °C)	J/gK	1.56 ± 0.08		1.61 ± 0.06
	$C_{p,g}$ (T = -50 °C)	J/gK	0.97 ± 0.03		0.95 ± 0.04
	$\Delta H_{cc}/\Delta H_m$	–	0.74	0.79	0.73
Density	ρ (T = 25 °C)	kg/m^3	1460 ± 10 (s) 1430 ± 10 (l)		
Thermal conductivity	k_l (T = 115 °C)	W/mK	0.35 ± 0.02		
	k_s (T = 29 °C)	W/mK	0.77 ± 0.03		

largest mass fraction of erythritol (W_{ery} = 0.8). Consequently, the volumetric latent heat storage capacity of CCM-A amounts to 250 MJ/m^3, which is based on the measured melting heat and liquid density. In comparison, CCM-B and CCM-C absorb lower amount of heat in melting, which is to be expected resulting from their lower mass fraction of erythritol (W_{ery} = 0.75).

Table 5 also tabulates the cold-crystallization heats of CCMs. The values cannot be directly compared to each other, since they depend on the temperature at which the phase change takes place:

$$\Delta H_{cc} = \Delta H_m - \int_{T_{cc}}^{T_m} (C_{p,l} - C_{p,s}) dT \quad (10)$$

where ΔH_m is melting heat and T_m the melting temperature. Nonetheless, given the stochastic nature of cold-crystallization, parallel values of ΔH_{cc} are repeatable with maximum standard deviation ± 8 J/g indicating predictable heat release behavior. During cold-crystallization, CCM-A, CCM-B and CCM-C release 74%, 79% and 73% of the latent heat, respectively. These comply with Eq. (10) assuming that the temperature of the DSC sample during cold-crystallization remains close to the defined T_{cc}. In principle, ΔH_{cc} of CCM can be increased according to Eq. (10) by elevating T_{cc}, which can be achieved by faster heating during initiation of cold-crystallization. It should be noted that the fraction of released latent heat does not represent the storage efficiency in reality, because sensible heat during cooling and initiation of cold-crystallization is not included.

Density and thermal conductivity were measured only for CCM-A, and they are listed in Table 5. Density of supercooled and solid CCM-A shows only a small difference at room temperature: 1430 kg/m^3 and 1460 kg/m^3. This is beneficial in heat storage applications because of the small changes of volume to the material during the phase change. However, the density of liquid CCM above T_m may differ from these values, which should be further investigated. Thermal conductivity of liquid CCM-A is within the range of the values that has been reported for pure erythritol (0.32–0.35 W/m K) [18,32,33,34]. On the other hand, comparison of solid state thermal conductivities is difficult, due to the wide range of values (0.39–0.89 W/m K) found for pure erythritol in the literature [18,32,33,34]. Nonetheless, CCM-A has a thermal conductivity at the high end of the range indicating that the polymer matrix has a negligible impact on the thermal conductivity of CCM-A.

3.2. Thermal chamber measurements

Thermal chamber measurement setup is used to determine cold-crystallization heat (ΔH_{cc}), cold-crystallization temperature (T_{cc}) and the maximum temperature of the sample during cold-crystallization (T_{max}). Based on the measured temperatures and heat transfer model, enthalpy-temperature curves for each measurement is calculated. Fig. 4 shows an example of the enthalpy-temperature curve. ΔH_{cc} and T_{cc} are estimated from the curve using the method described in Section 2.3.3. T_{max} is determined directly from the curve.

3.2.1. Cold-crystallization heat

Fig. 5 depicts the cold-crystallization heat of CCM samples stored for 1, 10, 30 and 97 days (composition A was also stored for 57 days). Each point in the figure represents an individual measurement made with the thermal chamber procedure. Further, the data set of the storage periods for the sample is not a continuous measurement. No reduction in ΔH_{cc} is observed for CCM-A samples after they are stored up to 97 days at 0 °C. The samples release consistently ~ 125 J/g of heat in cold-crystallization, which is over 70% of the melting heat measured by the DSC, indicating promising heat storage performance. In addition, no visual changes can be detected in the appearance of CCM-A-0-2 (sample from Batch 2 stored at 0 °C) after the storage period, as shown in Fig. 6. After the end of the 97 day storage, the sample begins to form minuscule grainy areas, which implies the beginning of slow crystallization. These results indicate that the molecular structure of CCM-A relaxes so slowly that the latent heat can be stored for at least 97 days at 0 °C without losing its heat content. However, as the storage period prolongs, possible crystallization (nucleation and growth) continues, as was visually implied in the sample images. Therefore, the crystallization tendency ought to be tested to confirm the stability of the supercooled state. The stability during cooling to the storage temperature in a refrigerator was confirmed by visual examination of the sample. None of the tested CCM samples showed signs of crystallization, meaning that grainy or opaque

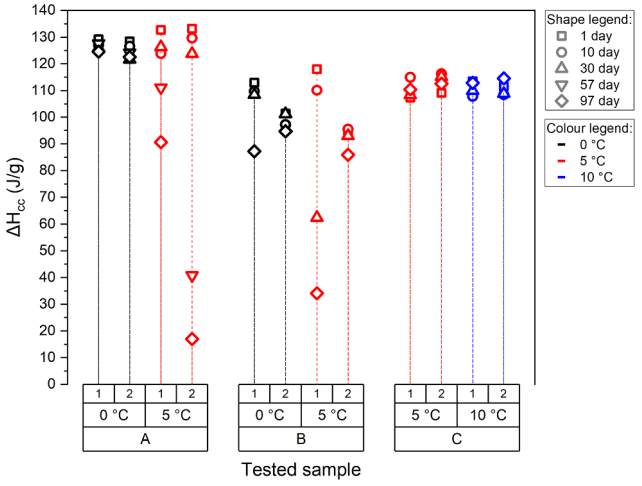

Fig. 5. Cold-crystallization heat of the tested samples. Letters A, B and C refer to the composition (see Table 1), 0 °C, 5 °C and 10 °C to the storage temperature and 1 and 2 to the composition's corresponding batch. Shape of the data point indicates the duration of the storage period and color indicates the storage temperature.

areas were not visible after cooling. To further this investigation, common characterization method, such as X-ray diffraction (XRD) ought to be employed to confirm the stability of the cooling process and the supercooled state.

As Fig. 5 shows, CCM-A samples exhibit a decrease of ~15–90 J/g in ΔH_{cc} after 57 days of storage at 5 °C. Furthermore, evident opaque areas form in CCM-A-5-2 sample after 57 days of storage (Fig. 6). This, together with the measurement of ΔH_{cc}, indicates partial crystallization of the sample during the storage. The crystallization (nucleation and growth) occurs slowly in a way that cold-crystallization heat decreases after 30 days. Crystallization of CCM-A-5-2 appears to begin already after 10 days of storage, as a several opaque areas are visible in the image after 30 days of storage (Fig. 6). Nonetheless, there is no clear decrease observed in ΔH_{cc} (Fig. 5). Most likely, opaque crystals occupy only a small volume fraction of the sample, demonstrating negligible effect on ΔH_{cc}. In any case, visual examination of the sample implies that the beginning of crystallization during storage period occurs earlier than the decrease in heat content.

Unlike CCM-A, supercooled CCM-B exhibits spontaneous crystallization at 0 °C or 5 °C, as indicated by lower ΔH_{cc} values in Fig. 5. ΔH_{cc} of most of the CCM-B samples decreases during the storage period, except that of CCM-B-0–2 (sample from Batch 2 stored at 0 °C). Nonetheless, CCM-B-0-1 releases 90 J/g of heat after 97 days of storage, which approximates to 80% of ΔH_{cc} measured after one to 30 days of storage. Measurements of CCM-B samples stored at 5 °C indicate deviation between the parallel samples. ΔH_{cc} of CCM-B-5-1 decreases 50% after 30 days of storage, while CCM-B-5-2 reduces only 10% after 97 days of storage (Fig. 5). Furthermore, the parallel samples of CCM-B deviate from each other around 10–15 J/g in ΔH_{cc} at the same storage temperature. The deviation between the parallel samples stems most likely from the preparation of the corresponding batches. CCM-B has a higher viscosity than other CCM compositions due to lower W_{ery} and X (Table 1). It has also a longer drying time. These factors could complicate the sample mixing and cause inhomogeneity of the batches.

CCM-C demonstrates a consistent ΔH_{cc} of around 110 J/g (Fig. 5), which totals to over 70% of ΔH_m measured by DSC. There is no noticeable variation in ΔH_{cc} between the samples stored up to 97 days at 5 °C and 10 °C. ΔH_{cc} of CCM-C is clearly lower as compared to CCM-A, due to the smaller mass fraction of erythritol. Nonetheless, the stability against crystallization is enhanced resulting from the larger mass fraction of the polymer. The demonstrated long-term stability of the supercooled CCM samples at moderate storage temperature (~10 °C) indicate that the cold-crystallizing polyol-polymer mixtures are suitable for large-scale long-term heat storage applications. Overall, the optimized CCM compositions show repeatable results for heat release, considering the accuracy of the measurement method and stochastic nature of crystallization.

It is fundamental, that the phase change characteristics remain similar in long-term use for several subsequent melting-crystallization cycles. Therefore, cycling stability was tested with two CCM-A samples in the temperature range of −20…+130 °C. Fig. 7 shows the results of the cycling measurements. The measurements indicate that when 50 melting-crystallization cycles is completed, cold-crystallization heat of ~125 J/g is consistently released. In addition, the appearance of the samples does not change during the cycling. These experiments indicate that the samples have repeatable long-term heat storage performance.

3.2.2. Cold-crystallization temperature levels

As we observed in the cold-crystallization heat analysis, crystallization occurs slowly at isothermal temperatures in the deeply supercooled state (close to T_g), but it accelerates when the temperature is increased. Therefore, T_{cc} describes the temperature, where crystallization begins to release sufficient amount of heat to increase the material temperature. As crystallization progresses under adiabatic conditions, the material temperature increases towards its melting temperature. Because nucleation is stochastic phenomenon, heating rate affects the crystallization. In addition, material temperature depends on the heat transfer rate between the sample and the environment (in this case, the heated oven air). Therefore, T_{cc} and the maximum temperature reached during cold-crystallization (T_{max}) are dependent upon the experimental system. Moreover, thermal chamber measurements cannot be directly compared to DSC measurements.

Figs. 8–10 plot the estimated cold-crystallization temperature (T_{cc}) and maximum temperature reached during cold-crystallization (T_{max}) for CCM-A to CCM-C, respectively. As can be seen in Fig. 8, T_{cc} of CCM-A stored for 1 and 10 days amounts to 30–34 °C for both storage temperatures (0 °C and 5 °C). In the case of 0 °C storage temperature, T_{cc} maintains at ~ 30 °C for all the storage periods (Fig. 8). On the other hand, T_{cc} of CCM-A stored at 5 °C is ~25 °C for the samples stored for 30 days or longer (Batch 1) and 57 days or longer (Batch 2). The consistent decrease of T_{cc} could be explained by the crystal formation during the storage period, inducing secondary nucleation and crystal growth. In addition, there is no induction period, which is the time period needed for the first crystal to appear [35], if crystals already exist in the sample. Therefore, the speed of crystallization increases earlier when crystals are formed during the storage period, unlike in the

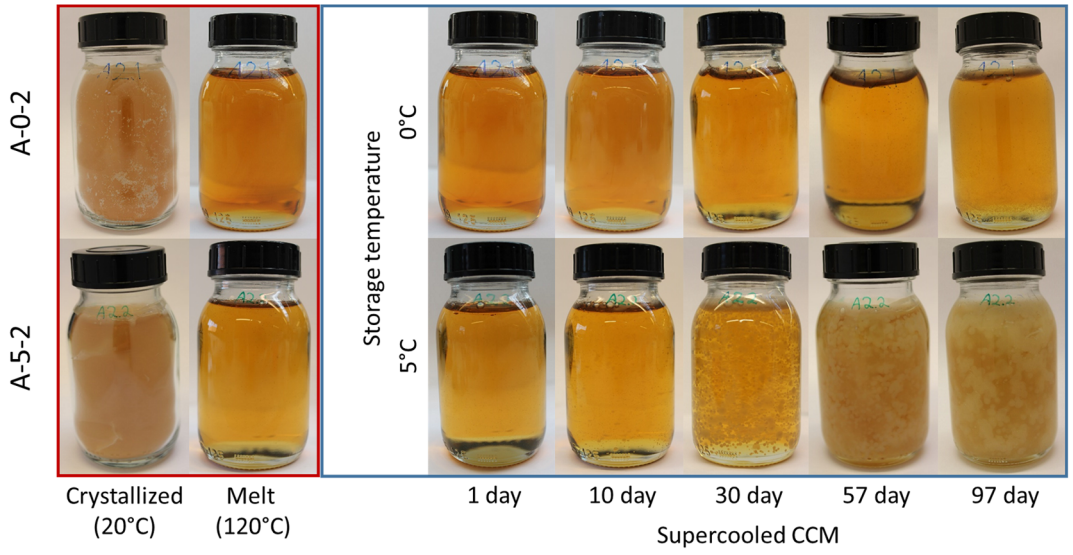

Fig. 6. Images of the supercooled samples after the storage period for composition A. Melt and crystallized samples are also included for comparison.

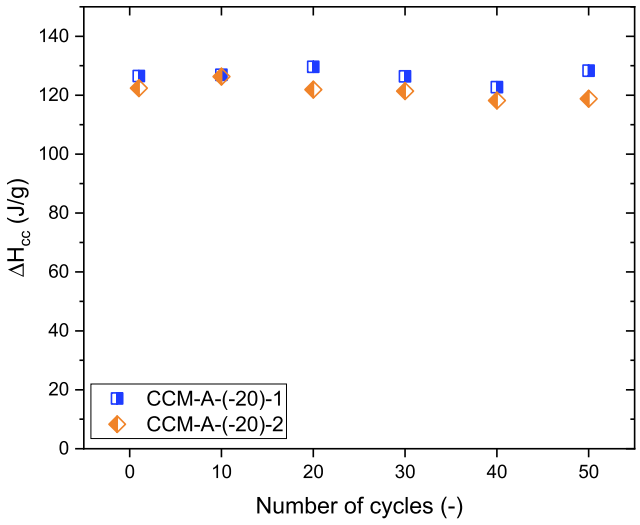

Fig. 7. Cold-crystallization heat of composition A for up to 50 melting-crystallization cycles. Storage temperature was −20 °C and storage period was 1 day.

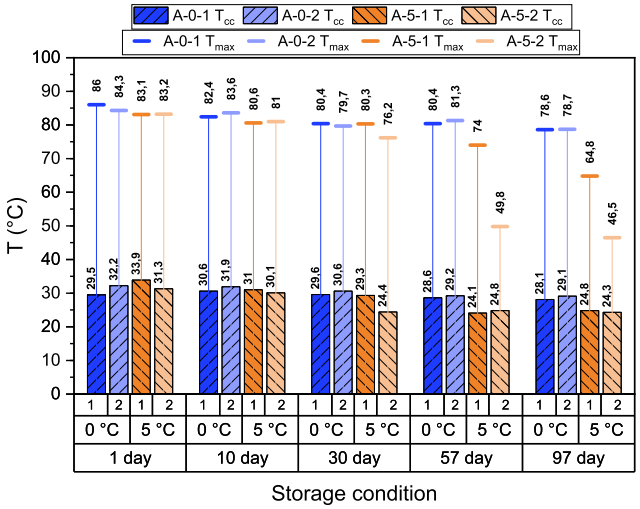

Fig. 8. Cold-crystallization temperature (T_{cc}) and maximum temperature reached during cold-crystallization (T_{max}) for composition A. Because the cold-crystallization is initiated by heating the sample with an oven at 50 °C for 6 h, the maximum temperature of the sample during the measurement rises towards 50 °C even if the sample does not release any heat.

samples without preformed crystals.

As shown in Fig. 9, T_{cc} of CCM-B totals to 38–44 °C when samples are stored for one day. From ten-day storage period onwards, T_{cc} of CCM-B Batch 1 samples begin to decrease, reaching the lowest value of 23 °C, while T_{cc} of CCM-B Batch 2 samples amounts to 41–44 °C for all the storage periods. This behavior is consistent with the observations made in the analysis of ΔH_{cc}, which indicated disparity between the batches.

As can be seen in Fig. 10, CCM-C has the highest T_{cc} of 51–54 °C after a one-day storage period. T_{cc} remains at 46–54 °C until 30-day storage period. However, it decreases to 40–47 °C after the samples are stored for 97 days. This implies the existence of small crystals in the samples, even though ΔH_{cc} of CCM-C did not decrease during the storage period. In addition, small opaque areas can be observed in the images of CCM-C samples stored for 97 days, suggesting the beginning of crystallization. These observations justify the longer storage period tests as necessary to identify the limits of the heat storing period at the storage temperatures of 10 °C and higher.

Results shown in Figs. 8–10 indicate that T_{cc} of 160-g scale CCM

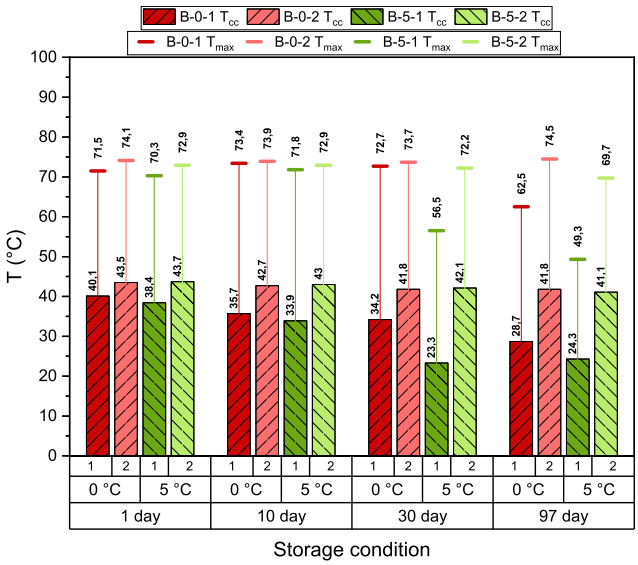

Fig. 9. Cold-crystallization temperature (T_{cc}) and maximum temperature reached during cold-crystallization (T_{max}) for composition B. Because the cold-crystallization is initiated by heating the sample with an oven at 55 °C for 6 h, the temperature of the sample during the measurement increases towards 55 °C even if the sample does not release any heat.

samples increase when X increases and W_{ery} decreases. The same behavior is also observed in DSC measurements for T_g and T_{cc} (Table 5) and in our previous DSC study [19]. This behavior occurs because of the increased molecular level interactions between the polymer and erythritol, which inhibit the crystallization tendency. ΔH_{cc} of CCM-A and CCM-C does not decrease when the samples were stored for three months at 18 °C and 16 °C above the T_g of the samples. This implies that CCM can store heat for long-term in the supercooled state at around T_g + 15 °C or below. More tests with other composition and several samples ought to be conducted in order to confirm the stable storage temperature for CCMs.

The maximum temperature reached during cold-crystallization of CCM (T_{max}) depends on T_{cc} and measurement conditions, such as the

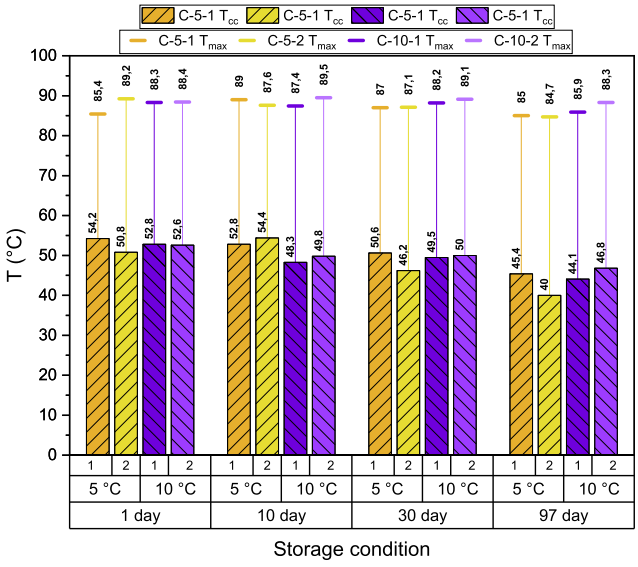

Fig. 10. Cold-crystallization temperature (T_{cc}) and maximum temperature reached during cold-crystallization (T_{max}) for composition C. Because cold-crystallization is initiated by heating the sample with an oven at 65 °C for 8 h, the temperature of the sample during the measurement increases towards 65 °C even if the sample does not release any heat.

Table 6
Comparison of specific heat of CCM measured by DSC and thermal chamber setup. The values include standard deviation.

Measurement type	Property	Unit	CCM-A	CCM-C
DSC	$C_{p,l}$ (T = 20 °C)	J/g K	2.16 ± 0.04	2.14 ± 0.03
	$C_{p,s}$ (T = 50 °C)	J/g K	1.56 ± 0.08	1.61 ± 0.06
Thermal chamber setup	$C_{p,l}$ (T = 20 °C)	J/g K	2.26 ± 0.09	2.14 ± 0.11
	$C_{p,s}$ (T = 50 °C)	J/g K	1.61 ± 0.07	1.67 ± 0.04

heating rate and heat losses to the environment. CCM-C reaches the highest T_{max} of 85–90 °C (Fig. 9), due to the high T_{cc} of 40–54 °C (Fig. 9). T_{max} of CCM-A and CCM-B are mostly in the range of 79–86 °C (Fig. 8) and 70–75 °C (Fig. 9), respectively, except for the storage periods where ΔH_{cc} begins to decrease. Deviations between compositions stem mostly from the different T_{cc} and ΔH_m as defined in Eq. (10). The heating rate of the samples is estimated to be 0.1–0.2 K/min for all compositions, thus we consider it having a negligible effect on T_{cc}.

For comparison, SAT has a melting temperature of 58 °C [11]. The 200 g bulk sample containing extra water was able to release a heat content around 170 J/g when measured once after a storage period of 100 days at room temperature [36]. Optimized CCM compositions show the maximum heat release temperature being 80–90 °C, which is a useful temperature range for many TES applications, such as domestic water heating and low temperature district heating. Furthermore, T_{max} and ΔH_{cc} (110–130 J/g, Fig. 5) of the optimized CCMs can be increased by increasing the heating rate (~0.1–0.2 K/min in thermal chamber measurement), as T_{cc} would take place at a higher temperature. In principle, heat can be released at T_m, which is between 106 and 108 °C (Table 5) for the tested CCMs according to DSC measurements. Long-term heat storage at this temperature level is attractive, as the storage unit could be connected to high temperature district heating systems without an auxiliary heat pump [37]. However, only a part of the latent heat could be available at this temperature level, as cold-crystallization heat converts into sensible heat as the temperature of the sample increases.

The values of specific heat measured with the thermal chamber setup are directly comparable with DSC. The values are listed in Table 6, and they correlate with one other. This supports the accuracy of the thermal chamber measurements, even though the standard deviation of thermal chamber measurements is larger than in the DSC measurements.

3.3. Storage performance indicators

There are three essential indicators that describe the performance of CCM-based heat storage: heat storage capacity, storage efficiency and heat charging/discharging rate. Volumetric heat storage capacity is a crucial parameter in storage applications, especially in domestic heating, that has limited available space. As this study examines the long-term heat storage capability of CCM, the storage capacity neglects the sensible heats for heating CCM to melting temperature and cooling CCM to storage temperature. Therefore, the latent heat determines the capacity of CCM. Consequently, CCM-A yields storage capacity of 250 MJ/m^3. Based on the results in Table 5, storage capacity of CCM-B and CCM-C approximate to ~200 MJ/m^3 and ~220 MJ/m^3, respectively. In comparison to PCMs for low and medium temperature applications, which typically range ~100–500 MJ/m^3 [38], CCM offers storage capacities in the mid-range. Therefore, improving the storage capacity of CCM through e.g. material selection, is one essential development area for the future research.

Comparison of storage capacities alone does not represent the entire operational behaviour, since conventional PCMs and sensible heat materials lose their capacity due to heat losses. Therefore, the storage efficiency is a key indicator for TES applications. The storage efficiency presented here assumes that all heat above T_{cc} is useful. Furthermore, the efficiency neglects the sensible heat absorbed during the heating of CCM to its melting temperature in charging mode, as well as the heat released on cooling CCM to storage temperature. This results in a storage efficiency in which cold-crystallization heat is divided by the melting heat and sensible heat for initiation of crystallization: $\varepsilon_{sto} = \Delta H_{cc}/(\Delta H_m + C_{p,l}(T_{cc} - T_{sto}))$. Storage efficiency of CCM-A stored at 0 °C and CCM-C stored at 10 °C from one to 97 days totals to ~55% and 50–60%, respectively. The advantage of CCM is that the efficiency remains the same for any storage period, given that spontaneous crystallization is prevented by the optimal storage conditions. Furthermore, if the low-temperature heat required for cold-crystallization is obtained from excess heat sources, for example from waste heat or the return line of the district heating network, the heat for initiation of crystallization can be subtracted from the efficiency. In this case, efficiencies for CCMA and CCM-C increase to 70–75%.

Real storage efficiencies are application dependent. Cooling of CCM to storage temperature could be implemented with natural cold sources. For example, the ground is cool year-round in cold climate areas and sometimes cold sources for small-scale applications are always available in the form of freezers. In addition, parts of the sensible heat of cooling could be used for short-term TES, as was demonstrated by a combined supercooling SAT and water storage system [14]. However, if free cooling was not available at the level of optimal storage temperature, external cooling energy would be necessary for long-term storage. This would decrease the storage efficiency resulting in unfeasible operation in long-term storage. Consequently, a stable storage temperature at the room temperature level would expand the applicability of CCM in residential applications, as low temperature cooling is not required. Furthermore, it would improve the viability of even longer storage periods for seasonal storage, e.g. half year to one year. Therefore, increasing the stable storage temperature is another essential aspect of developing CCM.

The charging and discharging rate of heat is significantly influenced by the heat transfer system in which the heat storage material is applied. In the thermal chamber setup, the discharging rate was estimated based on the rate of the temperature increase of CCM during cold-crystallization. Therefore, it describes the maximum heat release rate achievable in the applied system. Fig. 11 exemplifies the order of magnitude CCM-A is able to release. In the beginning of the cold-crystallization, the heat release rate is for the most part influenced by the thermal chamber heating (~4.6 W/kg$_{CCM}$). Nonetheless, the rate increases gradually until CCM-A reaches ~55 °C, after which the rate

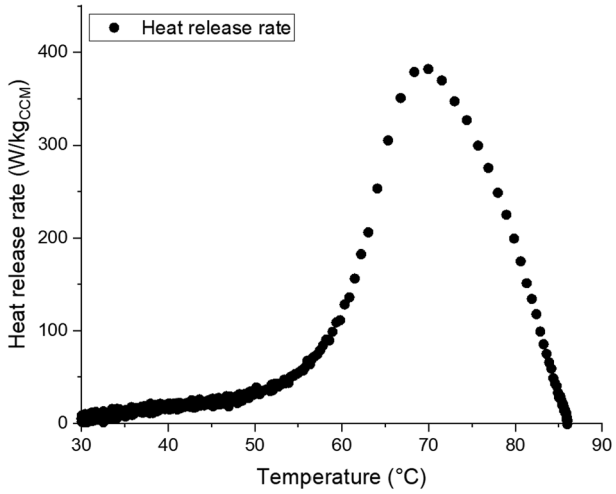

Fig. 11. An example of heat release rate as a function of CCM-A sample temperature measured with thermal chamber setup procedure. Each data point is measured with 10 s interval.

explodes and peaks at ~380 W/kg_{CCM}. This indicates that in order to optimize the heat release rate, crystallization should take place at 55 °C or above. Furthermore, quick heating to 55 °C when cold-crystallization is initiated would improve the heat release conditions. In this case, more latent heat is available at higher temperatures. All CCM-A samples do not achieve as high heat release rates. Instead, they maintain a constant rate for a longer period of time. Samples releasing ~130 J/g attain at least 100 W/kg_{CCM} for a five-minute period. These deviations demonstrate the variability of crystallization kinetics, which is contributed by the experimental setup and stochastic nature of cold-crystallization. CCM-C and CCM-B show lower heat release rates because they have a stable composition. Indeed, CCM-C (releasing 110 J/g) reaches its maximum heat release rate value of 70 W/kg_{CCM} and at least 15 W/kg_{CCM} for a 30 min period. CCM-B (releasing 100–110 J/g) releases heat at the lowest maximum rate of 30 W/kg_{CCM} with at least 10 W/kg_{CCM} for a 50 min period. Charging rate was estimated in the thermal chamber setup without the insulation shell. The average charging rate during melting of CCM-A amounts to 24 W/kg_{CCM}, which corresponds to the overall heat transfer coefficient of 16 W/m^2 K, when the thermal chamber heated the sample at the temperature of 126 °C. These results emphasize the relevance of charging/discharging rate in the further material development. Detailed analysis of the crystallization kinetics was descoped from this study.

4. Conclusions

This work demonstrates that cold-crystallizing materials (CCMs) are able to store heat reliably for long-term in bulk size (160 g). CCM consists of erythritol as a phase change material dispersed in cross-linked sodium polyacrylate matrix. The polymer matrix efficiently prevents spontaneous crystallization of erythritol polyol during cooling, and the latent heat of deeply supercooled or vitrified CCM can be stored at low temperatures for long-term heat storage purposes. The latent heat is released by cold-crystallization when the material is re-heated.

We use experimental temperature data from the thermal chamber setup alongside a one-dimensional transient heat conduction model to estimate the cold-crystallization heat of CCM compositions (160 g samples). Three compositions of CCM with varying mass fractions of erythritol (W_{ery}) and neutralization degrees of sodium polyacrylate (X) were chosen for this study based on scale-up experiments: CCM-A (W_{ery} = 0.8, X = 1); CCM-B (W_{ery} = 0.75, X = 0.85) and CCM-C (W_{ery} = 0.75, X = 1). CCM samples are first melted, and then stored in the supercooled state at 0 °C, 5 °C and 10 °C up to 97 days. The long-term heat storage behaviour of CCM-A samples stored at 0 °C show high reliability; no decrease in cold-crystallization heat (ΔH_{cc} = 125 J/g) is observed during the storage period up to 97 days. However, the storage temperature of 5 °C is too high for the long-term storage: the heat content began to reduce after 30 days of storage resulting from slow crystallization. Nevertheless, reliable long-term storage at higher storage temperatures is achieved by decreasing the mass fraction of erythritol from 80 wt-% (CCM-A) to 75 wt-% (CCM-C). Indeed, the cold-crystallization heat of CCM-C (ΔH_{cc} = 110 J/g) stored at 10 °C do not decrease at all during the storage periods up to 97 days. Therefore, the tested CCMs could realize an efficient storage for even longer storage periods.

The maximum temperature reached during cold-crystallization of CCM-A and CCM-C amounts to 80–90 °C, which would be a sufficient temperature level for domestic water heating. In principal, heat release temperature level of 106–108 °C could be achieved, if cold-crystallization temperature could be increased to a sufficiently high level. In this case, the stored heat could be provided even for district heating.

The demonstrated ability of CCMs to store heat reliably for several months at moderate storage temperatures in bulk size is advantageous for small and intermediate size heat storage applications, such as residential heating. CCM is also promising for district heating, if the cold-crystallization temperature could be increased further. The material has excellent properties for long-term heat storage purposes, as over 70% of the latent heat can be released in cold-crystallization. CCM-A shows a volumetric heat storage capacity of 250 MJ/m^3 and a sufficient crystallization speed for applications in the heat release rate examination. These material properties in bulk size provide valuable insights on design parameters and operational behavior for larger-scale applications, which ought be the next stage of the scale-up.

CRediT authorship contribution statement

Konsta Turunen: Conceptualization, Methodology, Software, Validation, Formal analysis, Investigation, Writing - original draft, Visualization, Project administration, Funding acquisition. **Maryam Roza Yazdani:** Conceptualization, Methodology, Validation, Writing - review & editing, Visualization. **Salla Puupponen:** Conceptualization, Writing - review & editing, Funding acquisition. **Annukka Santasalo-Aarnio:** Conceptualization, Writing - review & editing, Supervision, Visualization. **Ari Seppälä:** Conceptualization, Methodology, Investigation, Writing - review & editing, Supervision, Project administration, Funding acquisition.

Declaration of Competing Interest

The authors declare that they have no known competing financial interests or personal relationships that could have appeared to influence the work reported in this paper.

Acknowledgements

The research received funding from the Maj and Tor Nessling Foundation (201900332) and the Business Finland (HeatStock-project). The authors wish to acknowledge B.Sc. Markus Laitinen for his contribution in density measurements.

References

[1] Shah SK, Aye L, Rismanchi B. Seasonal thermal energy storage system for cold climate zones: A review of recent developments. Renew Sustain Energy Rev 2018;97:38–49. https://doi.org/10.1016/j.rser.2018.08.025.
[2] Novo AV, Bayon JR, Castro-Fresno D, Rodriguez-Hernandez J. Review of seasonal heat storage in large basins: Water tanks and gravel–water pits. Appl Energy 2010;87:390–7. https://doi.org/10.1016/J.APENERGY.2009.06.033.
[3] Kousksou T, Bruel P, Jamil A, El Rhafiki T, Zeraouli Y. Energy storage: Applications and challenges. Sol Energy Mater Sol Cells 2014;120:59–80. https://doi.org/10.1016/j.solmat.2013.08.015.
[4] Scapino L, Zondag HA, Van Bael J, Diriken J, Rindt CCM. Sorption heat storage for long-term low-temperature applications: A review on the advancements at material and prototype scale. Appl Energy 2017;190:920–48. https://doi.org/10.1016/j.apenergy.2016.12.148.
[5] Debenedetti PG. Metastable liquids - concepts and principles. New Jersey, USA: Princeton University Press; 1996.
[6] Sandnes B, Rekstad J. Supercooling salt hydrates: Stored enthalpy as a function of temperature. Sol Energy 2006;80:616–25. https://doi.org/10.1016/J.SOLENER.2004.11.014.
[7] Safari A, Saidur R, Sulaiman FA, Xu Y, Dong J. A review on supercooling of phase change materials in thermal energy storage systems. Renew Sustain Energy Rev 2017;70:905–19. https://doi.org/10.1016/j.rser.2016.11.272.
[8] Hasan Zahir M, Mohamed SA, Saidur R, Al-sulaiman FA. Supercooling of phase-change materials and the techniques used to mitigate the phenomenon. Appl Energy 2019;240:793–817. https://doi.org/10.1016/j.apenergy.2019.02.045.
[9] Cronenberg C, Szczawinski MSB. Device for retaining heat in foods, &c. US Patent No. 549,959, n.d.
[10] Sandnes B. The physics and the chemistry of the heat pad. Am J Phys 2008;76:546–50. https://doi.org/10.1119/1.2830533.
[11] Sharma A, Tyagi VV, Chen CR, Buddhi D. Review on thermal energy storage with phase change materials and applications. Renew Sustain Energy Rev 2009;13:318–45. https://doi.org/10.1016/j.rser.2007.10.005.
[12] Dannemand M, Johansen JB, Kong W, Furbo S. Experimental investigations on cylindrical latent heat storage units with sodium acetate trihydrate composites utilizing supercooling. Appl Energy 2016;177:591–601. https://doi.org/10.1016/j.apenergy.2016.05.144.
[13] Dannemand M, Dragsted J, Fan J, Johansen JB, Kong W, Furbo S. Experimental investigations on prototype heat storage units utilizing stable supercooling of sodium acetate trihydrate mixtures. Appl Energy 2016;169:72–80. https://doi.org/

10.1016/J.APENERGY.2016.02.038.
[14] Englmair G, Furbo S, Dannemand M, Fan J. Experimental investigation of a tank-in-tank heat storage unit utilizing stable supercooling of sodium acetate trihydrate. 114709 Appl Therm Eng 2020;167. https://doi.org/10.1016/j.applthermaleng.2019.114709.
[15] Dannemand M, Schultz JM, Johansen JB, Furbo S. Long term thermal energy storage with stable supercooled sodium acetate trihydrate. Appl Therm Eng 2015;91:671–8. https://doi.org/10.1016/J.APPLTHERMALENG.2015.08.055.
[16] Hirano S, Saitoh TS. Long-term performance of latent heat thermal energy storage using supercooling. Proc ISES World Congr 2007 2008;Vol. I-V:2741–5. 10.1007/978-3-540-75997-3_553.
[17] Seppälä A, Meriläinen A, Wikström L, Kauranen P. The effect of additives on the speed of the crystallization front of xylitol with various degrees of supercooling. Exp Therm Fluid Sci 2010;34:523–7. https://doi.org/10.1016/j.expthermflusci.2009.11.005.
[18] Puupponen S, Mikkola V, Ala-Nissila T, Seppälä A. Novel microstructured polyol–polystyrene composites for seasonal heat storage. Appl Energy 2016;172:96–106. https://doi.org/10.1016/J.APENERGY.2016.03.023.
[19] Puupponen S, Seppälä A. Cold-crystallization of polyelectrolyte absorbed polyol for long-term thermal energy storage. Sol Energy Mater Sol Cells 2018;180:59–66. https://doi.org/10.1016/j.solmat.2018.02.013.
[20] Nakano K, Masuda Y, Daiguji H. Crystallization and melting behavior of erythritol in and around two-dimensional hexagonal mesoporous silica. J Phys Chem C 2015;119:4769–77. https://doi.org/10.1021/jp510048g.
[21] Wang Z, Roffey A, Losantos R, Lennartson A, Jevric M, Petersen AU, et al. Macroscopic heat release in a molecular solar thermal energy storage system. Energy Environ Sci 2018;12:187–93. https://doi.org/10.1039/c8ee01011k.
[22] Mansø M, Petersen AU, Wang Z, Erhart P, Nielsen MB. Moth-poulsen K. Molecular solar thermal energy storage in photoswitch oligomers increases energy densities and storage times. Nat Commun 2018;9. https://doi.org/10.1038/s41467-018-04230-8.
[23] Han GGD, Li H, Grossman JC. Optically-controlled long-term storage and release of thermal energy in phase-change materials. Nat Commun 2017;8. https://doi.org/10.1038/s41467-017-01608-y.
[24] Iwase K, Nagano Y, Yoshikawa I, Houjou H, Yamamura Y, Saito K. Cold crystallization in Schiff-base nickel(II) complexes derived from three toluidine isomers. J Phys Chem C 2014;118:27664–71. https://doi.org/10.1021/jp5081516.
[25] JCGM. Joint committee for guides in metrology. Evaluation of measurement data — Guide to the expression of uncertainty in measurement. JCGM 100 2008.
[26] Perry RH, Green DW. Perry's chemical engineers' handbook. seventh ed. Australia: McGraw-Hill; 1998.
[27] VDI-Gesellschaft Verfahrenstechnik und Chemieingenieurwesen (GVC), editor. VDI Heat Atlas. Second Edi. Berlin Heidelberg: Springer-Verlag; 2010. 10.1007/978-3-540-77877-6.
[28] Yingping Z, Yi J, Yi J. A simple method, the T-history method, of determining the heat of fusion, specific heat and thermal conductivity of phase-change materials. Meas Sci Technol 1999;10:201–5.
[29] Badenhorst H, Cabeza LF. Critical analysis of the T-history method: A fundamental approach. Thermochim Acta 2017;650:95–105. https://doi.org/10.1016/j.tca.2017.02.005.
[30] Tan P, Brütting M, Vidi S, Ebert H, Johansson P, Jansson H, et al. Correction of the enthalpy-temperature curve of phase change materials obtained from the T-History method based on a transient heat conduction model. Int J Heat Mass Transf 2017;105:573–88. https://doi.org/10.1016/j.ijheatmasstransfer.2016.10.001.
[31] Tan P, Brütting M, Vidi S, Ebert H, Johansson P, Kalagasidis AS. Characterizing phase change materials using the T-History method: On the factors in fluencing the accuracy and precision of the enthalpy-temperature curve. Thermochim Acta 2018;666:212–28. https://doi.org/10.1016/j.tca.2018.07.004.
[32] Gunasekara SN, Chiu JN, Martin V, Hedström P. The experimental phase diagram study of the binary polyols system erythritol-xylitol. Sol Energy Mater Sol Cells 2018;174:248–62. https://doi.org/10.1016/j.solmat.2017.08.005.
[33] Kakiuchi H, Yamazaki M, Yabe M, Chihara S, Terunuma T, Sakata Y, et al. A study of erythritol as phase change material. IEA Annex 10-PCMs Chem. React. Therm. Energy Storage, Second Work. Sofia, Chemical Engineering and Technology, Royal Institute of Technology; 1998.
[34] Höhlein S, König-Haagen A, Brüggemann D. Thermophysical characterization of MgCl2·6H2O, xylitol and erythritol as phase change materials (PCM) for latent heat thermal energy storage (LHTES). Materials (Basel) 2017;10:1–15. https://doi.org/10.3390/ma10040444.
[35] Mullin JW. Crystallization. 4th ed. Oxford: Butterworth-Heinemann; 2001.
[36] Kong W, Dannemand M, Johansen JB, Fan J, Dragsted J, Englmair G, et al. Experimental investigations on heat content of supercooled sodium acetate trihydrate by a simple heat loss method. Sol Energy 2016;139:249–57. https://doi.org/10.1016/j.solener.2016.09.045.
[37] Guelpa E, Verda V. Thermal energy storage in district heating and cooling systems: A review. Appl Energy 2019;252. https://doi.org/10.1016/j.apenergy.2019.113474.
[38] Pereira da Cunha J, Eames P. Thermal energy storage for low and medium temperature applications using phase change materials – A review. Appl Energy 2016;177:227–38. https://doi.org/10.1016/j.apenergy.2016.05.097.